Investigation of lateral modulation in antimonide superlattices

R. L. Forrest,[1,*] J. Throckmorton,[1] C. L. Canedy,[2] G. Boishin,[2,†] I. Vurgaftman,[2] J. R. Meyer,[2] and L. J. Whitman[2,‡]
[1]*University of Houston, Houston, Texas 77204, USA*
[2]*Naval Research Laboratory, Washington, D.C. 20375, USA*
(Received 10 December 2010; published 16 March 2011)

Lateral structure is investigated in two antimonide superlattices using x-ray diffraction. We report periodic lateral modulation in AlSb/AlAs digital superlattices, while no lateral modulation is observed in similar InAs/Al(In)Sb digital superlattices. By fitting the diffraction data with dynamical diffraction theory we are able to determine the strain in each layer and at the interfaces. The findings are consistent with recent predictions of the critical thickness for three-dimensional growth.

DOI: 10.1103/PhysRevB.83.115320 PACS number(s): 61.05.cp, 68.65.Cd, 81.05.Ea

I. INTRODUCTION

Lateral modulation is the spontaneous formation of a periodic variation in structure or alloy composition perpendicular to the growth direction in an epitaxial structure. It has been observed in many epitaxially grown III–V semiconductor alloys, occurring during the homogenous growth of III–V alloys and in superlattices grown by both molecular beam epitaxy and metal-organic vapor phase epitaxy.[1–6] In zinc blende structures lateral modulation typically occurs along one of the [110] directions. The occurrence of lateral modulation is associated with strain and growth kinetics.[7–9] It begins when strain is relieved through elastic surface undulations, typically in layers much thinner than the critical thickness for dislocation formation. These undulations may either grow or be damped, depending on the properties of the layers and on the growth kinetics. Under the right conditions, the undulations form a periodic lateral structure. Lateral modulation is interesting both as an example of self-assembly, and for its potential usefulness in applications.[10–12]

II. EXPERIMENT

We have investigated the lateral structure of two different strain-balanced antimonide superlattices: AlSb/AlAs and InAs/AlInSb. Both of the superlattice systems studied here were incorporated as buffer layers in type-II "*W*" quantum well mid-IR lasers grown by molecular beam epitaxy on (100) GaSb substrates. Since these particular structures were grown as structural and optical calibration samples for laser optimization efforts at the Naval Research Laboratory,[13–17] they did not have all of the layers or thicknesses required for fully functional devices. Samples in Set 1 were designed to contain an 80.7 Å AlSb/5.7 Å AlAs "digital alloy" superlattice buffer layer, followed by a five-period 18.2 Å InAs/34.2 Å $Ga_{0.7}In_{0.3}Sb$/18.2 Å InAs/234.3 Å $AlAs_{0.106}Sb_{0.894}$ "*W*" quantum well (∼1524 Å), a seven-period 24.5 Å AlSb/3.3 Å AlAs digital-alloy barrier (∼195 Å), and a 150 Å GaSb cap layer. The buffer superlattice in Sample 1A is 122 periods (∼10,000 Å) thick, while that in Sample 1B is 58 periods (∼5000 Å) thick. For further growth details, see Refs. 16 and 17.

Set 2 samples were designed to contain an 18.8 Å InAs/18.8 Å $Al_{0.95}In_{0.05}Sb$ superlattice buffer layer, followed by 0.4 μm of GaSb, a five-period 21.2 Å InAs/30 Å $Ga_{0.92}In_{0.08}Sb$/21.2 Å InAs/40 Å $Al_{0.35}Ga_{0.65}Sb$ "W" quantum well (∼562 Å), and a 200 Å GaSb cap layer. The samples in this set, 2A, 2B, and 2C, have buffer thicknesses of 5000 Å, 15,000 Å, and 15,000 Å, respectively. The growth details for these structures are similar to those described in Ref. 15.

We performed high-resolution x-ray diffraction measurements on a four-circle diffractometer using Cu $K\alpha_1$ radiation to characterize the samples' superlattice and lateral structures. Radial scans and reciprocal space maps (RSMs) were acquired about the (004) and (224) Bragg peaks. RSMs were done in both the (110) and $(\bar{1}10)$ planes to identify any lateral structure in either direction. Cross-sectional scanning tunneling microscopy (XSTM) images were acquired in ultrahigh vacuum following procedures described previously.[18]

An RSM about the (224) peak of sample 1B is shown in Fig. 1, with axes labeled by the Miller indices in reciprocal lattice units (rlu). The RSMs from samples 1A and 1B look similar. Since both the buffer and "*W*" superlattices are strain-balanced to lattice match the GaSb substrate, their central peaks coincide with the GaSb (224) peak. The +1 and −1 satellite (SL) peaks from the AlSb/AlAs superlattice buffer are evident, as well as several SL peaks from the "*W*" superlattice (not labeled in Fig. 1). Peaks from the thin barrier superlattice are indistinguishable from those of the buffer. The epitaxial layers are fully strained to the GaSb substrate, as all SL peaks lie along *L*, that is (001), in this "off-axis" RSM.

Lateral satellite peaks can be seen about both the SL +1 and SL − 1 buffer peaks, but not the central SL0. This indicates a purely structural periodic lateral modulation in the buffer superlattice. On the other hand, no lateral peaks accompany the weaker "*W*" SL peaks. The lateral peaks are clearly evident in Fig. 1(b), which shows an enlarged view of the (224) buffer SL − 1 peak. Lateral satellites are also visible about the (004) and (002) buffer SL peaks. No lateral peaks were present in the perpendicular (110) plane. The positions of the lateral satellites for the AlSb/AlAs superlattice buffers in samples 1A and 1B indicate lateral modulation periods of 1720 ± 20 Å and 1050 ± 30 Å, respectively.

Figure 2 shows an XSTM image of the AlSb/AlAs buffer in sample 1B. A wave-like feature is clearly visible. The image also appears to show a second set of wave troughs near the top right. The spacing between the troughs corresponds to a lateral period of about 540 ± 10 Å, or about half of the 1050 ± 30 Å period measured by x-ray diffraction. (Because this was the largest image acquired, we were unable to characterize

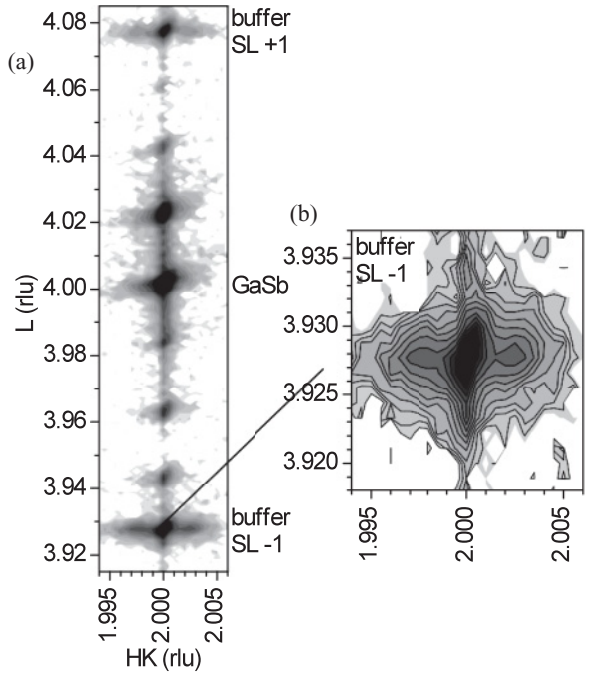

FIG. 1. (a) RSM about the (224) reciprocal lattice point in the AlSb/AlAs buffer sample 1B showing buffer and *W* SL peaks, and lateral peaks about the buffer SL peaks. The HK axis has been expanded to show detail. (b) Expanded RSM about the buffer SL − 1 peak showing the lateral peaks at HK = 2 ± 0.0025 rlu. The axes are to scale.

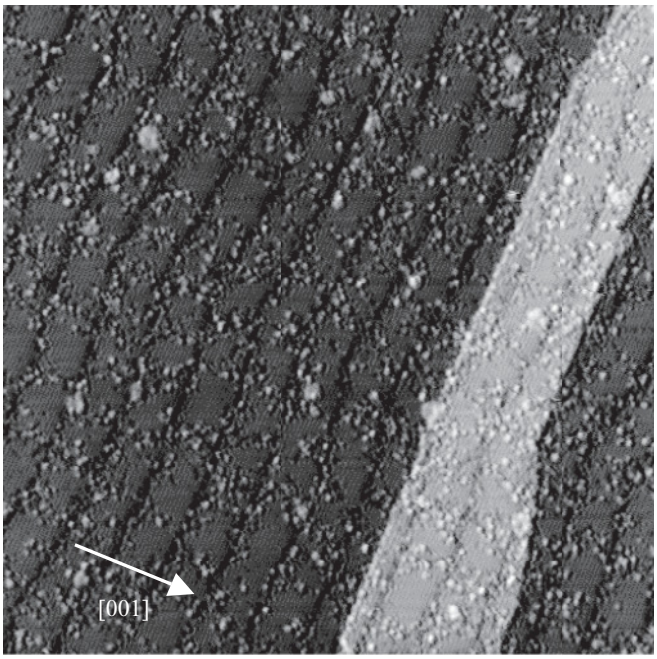

FIG. 2. Cross-sectional scanning tunneling micrograph image showing the wavy lateral modulation in an AlSb/AlAs buffer. The size of the image is 100 nm × 100 nm. The [001] growth direction is indicated. The light gray section is a monoatomic cleavage terrace.

multiple lateral modulation periods.) The discrepancy could be due to variations within the sample, or to a more complicated lateral structure associated with a tilt of the modulation.[5,7] X-ray diffraction measurements give the average period for the entire measured sample volume, which includes the entire height vertically and a few mm^2 laterally. The XSTM image confirms that the lateral modulation is purely structural rather than compositional, with all layers modulating in phase.

Figure 3 shows a radial scan of sample 1B through the (004) Bragg peak. Several superlattice peaks from both the buffer and "*W*" superlattices can be seen. These data were fit to determine the composition and thickness of the layers in the sample. Since our interest is in the laterally modulated AlSb/AlAs buffer, only the buffer superlattice was fully modeled. An approximate simulation of the intensity from the "*W*" superlattice was calculated and added as background to the buffer layer intensity to improve the χ^2 of the overall result. We simulated the diffracted intensity from the buffer layers using dynamic scattering theory and a χ^2 simplex fitting algorithm.[19] Dynamical theory is appropriate for the buffers due to their 5000 to 10 000 Å thicknesses, making multiple reflections likely. The dynamical simulation was performed by the x-ray Server, http://x-server.gmca.aps.anl.gov/automation.html, which was called from within a local χ^2 fitting program. The fitting process is described in detail in Stepanov *et al.*[20]

In fitting the nominal two-layer superlattices we allowed for four layers: $AlAs_{y1}Sb_{1-y1}(t_1)/AlAs_{y2}Sb_{1-y2}(t_2)/AlAs_{y3}Sb_{1-y3}(t_3)/AlAs_{y4}Sb_{1-y4}(t_4)$. Here y_i is the group-V composition and t_i is the thickness of the ith layer. Group V mixing is allowed in all layers, and the extra layers are included to simulate interdiffusion at the interfaces. The thicknesses and compositions were variables in the fitting process. The interdiffusion layers were assumed to be thin; t_2 and t_4 were constrained to be less than 12 Å. We assumed that the compositions were related to the relaxed lattice constants according to Vegard's law, and the relaxed and strained lattice constants are related through the standard elastic relations. When the composition y_i was near 0 or 1, binary elastic

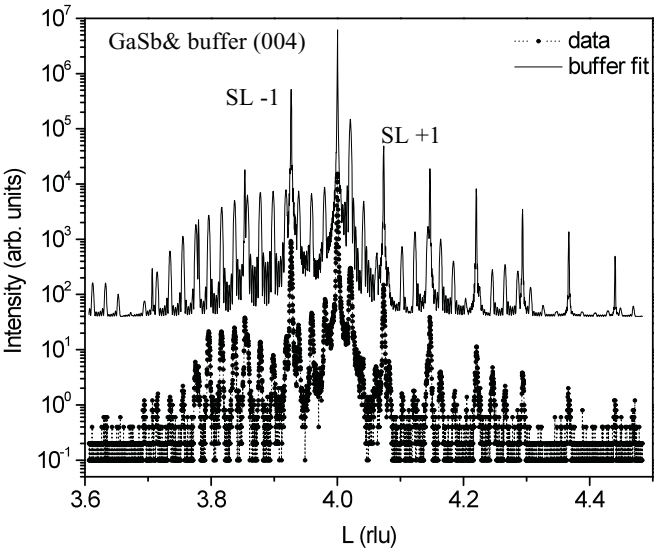

FIG. 3. Radial x-ray diffraction scan through the (004) Bragg peak in the AlSb/AlAs buffer sample 1B showing buffer and W SL peaks. Experimental data—line with points, simulation— line, offset vertically for clarity.

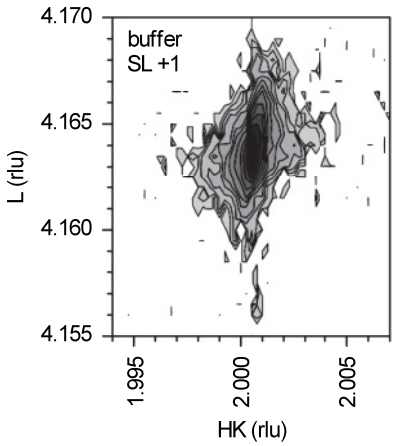

FIG. 4. RSM about the InAs/Al(In)Sb buffer sample 2B's (224) SL +1 peak. There are no lateral peaks. The axes are to scale.

stiffness constants were used, while a linear interpolation was used for y_i near 0.5.[21] The best fit to the data for sample 1B is shown as the solid line in Fig. 3. The fitted curve has been offset vertically for clarity.

RSMs were also made for the three Set 2 samples. A typical RSM about the (224) buffer SL +1 peak is shown in Fig. 4, corresponding to sample 2B. No lateral peaks were observed in either (110) plane for any of the Set 2 InAs/Al(In)Sb buffer samples, confirming that the Set 2 samples do not contain lateral modulation.

A radial scan through the (004) Bragg peak of sample 2B is shown in Fig. 5 as a curve with points, with the best fit of the buffer structure shown as a curve without points, offset for clarity. The Set 2 buffers were fit with the dynamical simulation and fitting algorithm described above, as the buffers have thicknesses from 5000 to 15 000 Å. As can be seen from Fig. 5, we did not need to simulate the active "*W*" superlattices to get a good fit for the Set 2

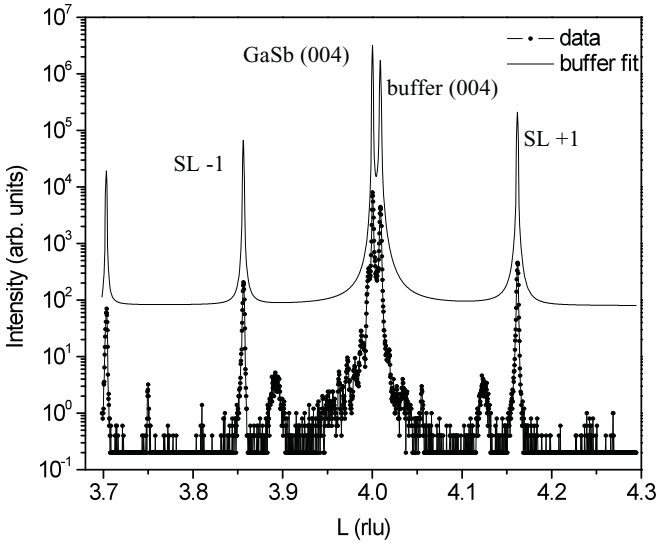

FIG. 5. Radial x-ray diffraction scan through the (004) Bragg peak in the InAs/Al(In)Sb buffer sample 2B showing buffer and W SL peaks. Experimental data—line with points, simulation—line, offset vertically for clarity.

TABLE I. Best-fit structure of Set 1 superlattice buffers, including thickness (t), alloy composition (y), and strain (ε) in each of the simulated layers. The critical thickness for modulation, t_c, and the vertical superlattice period, Λ, are also listed. The intended structure was 80.7 Å AlSb/5.7 Å AlAs, with $\Lambda = 82$ Å.

	Sample 1A			Sample 1B			
Layer	t (Å)	y	ε (%)	t (Å)	y	ε (%)	t_c (Å)
$AlAs_ySb_{1-y}$	5.1	0.89	−6.3	4.3	1.0	−7.1	2
$AlAs_ySb_{1-y}$	4.0	0.34	−2.0	2.1	0.68	−4.7	4
$AlAs_ySb_{1-y}$	71.8	0.01	+0.6	76.7	0.01	+0.6	200
Λ	80.9			83.1			

samples. Our Set 2 model allowed for the four layers $InAs_{y1}Sb_{1-y1}(t_1)/InAs_{y2}Sb_{1-y2}(t_2)/Al_{x3}In_{1-x3}As_{y3}Sb_{1-y3}(t_3)/Al_{x4}In_{1-x4}As_{y4}Sb_{1-y4}(t_4)$. Here x_i is the group-III composition, y_i is the group-V composition, and t_i is the thickness of the ith layer. As for the Set 1 fits, group-V mixing is allowed in all layers and the additional layers are intended to model interdiffusion at the interfaces. While both fractional compositions, x and y, in a quaternary alloy weakly effect the relative intensities of the various peaks, they are most strongly correlated to a single value, the lattice constant of the layer. Therefore, there is greater uncertainty in the values of x and y when both are to be fit from x-ray diffraction data alone. To minimize the uncertainty in x and y of the two quaternary layers, the set 2 data were first fit with only two layers, $InAs_{y1}Sb_{1-y1}(t_1)/Al_{x3}In_{1-x3}As_{y3}Sb_{1-y3}(t_3)$. The value of y_3 determined from this fit was then used as a fixed parameter in the four-layer model. Furthermore, since intermixing of group-III atoms is less prevalent than that of group-V atoms, we constrained the group-III composition in the quaternary interdiffusion layer 4 to be the same as that in the preceding layer, i.e., $x_3 = x_4$.

III. MODELING RESULTS AND DISCUSSION

The best fits for the Set 1 samples are listed in Table I. In both Set 1 samples there is a small amount of As in the thick AlSb layer, which corresponds to the bright clumps seen in the thick AlSb layers in the XSTM image in Fig. 2. The best fits for both Set 1 samples correspond to a three-layer structure, with an interdiffusion layer between the thick Al(As)Sb and the thin AlAs(Sb). These results are consistent with XSTM observations of mixing at AlAs-on-AlSb interfaces seen in Fig. 2 and in similar samples.[17] The misfit strain in each layer is also listed in Table I, where we define the misfit strain as $\varepsilon = (a_0 - a_s)/a_s \times 100\%$. Here a_0 is the relaxed lattice constant of the layer and a_s is the lattice constant of the GaSb substrate.

The best fits for the Set 2 samples are listed in Table II. In the fits of all three Set 2 buffers there is no group V mixing in the InAs layer, but it is followed by an approximately one monolayer InAsSb interdiffusion layer. The composition of sample 2A's $Al_{0.90}In_{0.10}Sb$ layer differs from the intended $Al_{0.95}In_{0.05}Sb$, but samples 2B and 2C are on target. The fits for samples 2B and 2C also include an AlInAsSb interdiffusion layer (less than 1 monolayer thick) above the AlInSb layer.

The Set 1 AlSb/AlAs superlattices exhibit lateral modulation, while there is none in the Set 2 InAs/Al(In)Sb

TABLE II. Best-fit structure of Set 2 superlattice buffers, including thickness (t), alloy composition (x, y), and strain (ε) in each of the simulated layers. The critical thickness for modulation, t_c, and the vertical superlattice period, Λ, are also listed. The intended structure was 18.8 Å InAs/18.8 Å $Al_{0.95}In_{0.05}Sb$, with $\Lambda = 37$ Å.

	Sample 2A			Sample 2B			Sample 2C			
Layer	t (Å)	x, y	ε (%)	t (Å)	x, y	ε (%)	t (Å)	x, y	ε (%)	t_c (Å)
$Al_xIn_{1-x}As_ySb_{1-y}$	0			2.1	$x = 0.94$ $y = 0.38$	−1.9	1.2	$x = 0.95$ $y = 0.51$	−3.0	4
$Al_xIn_{1-x}As_ySb_{1-y}$	8.5	$x = 0.90$ $y = 0$	+1.2	9.0	$x = 0.94$ $y = 0$	+1.0	10.0	$x = 0.95$ $y = 0.2$	+0.8	200
$InAs_ySb_{1-y}$	1.9	$y = 0.43$	+3.3	2.8	$y = 0.47$	+3.0	2.1	$y = 0.23$	+4.7	7
$InAs_ySb_{1-y}$	26.9	$y = 0$	−0.6	25.9	$y = 0$	−0.6	26.6	$y = 0$	−0.6	247
Λ	37.3			39.8			39.9			

superlattices. To the authors' knowledge, this is the first report of AlSb/AlAs superlattices with lateral modulation. This may also be the first report of purely structural lateral modulation in a superlattice. The finding is qualitatively consistent with work by Shilkrot *et al.*,[9] who predicted that a relatively narrow range of strained-layer superlattice growth conditions can lead to in-phase layer undulations and purely structural modulation. As they pointed out, however, it is difficult to apply their predictions to real experimental systems, and it is not clear whether our superlattices would fall within their predicted growth conditions corresponding to purely structural modulation.

The observed lateral modulation, and lack thereof, is also consistent with recent predictions of the critical thickness for modulated or three-dimensional growth.[22] For a film that relaxes due to the formation of a triangular surface, Sasaki *et al.* derived the following critical thickness based on thermodynamic considerations:

$$t_c = \frac{5(1-\nu_f)\lambda}{2E_f\left[\ln\left(\frac{a_f}{a_s}\right)\right]^2}\tan\theta. \quad (1)$$

Here f refers to the film, s refers to the substrate, λ is the surface energy per unit area of a flat film, θ is the angle between the base and the side of the triangular profile, E is Young's modulus, and ν is Poisson's ratio. All of the variables in Eq. (1) can be determined for our films except the surface energy density. Following Sasaki *et al.*, we estimate the energy density as $\lambda = \frac{2}{a_f a_{sub}} k_B T$ for the flat [100] surface, where $k_B T$ is the thermal energy at the melting point of the film. The critical thicknesses calculated using (1)) are listed in Tables I and II.

In the Set 1 samples, which contain lateral modulation, the ∼5 Å Al(As)Sb layer exceeds the critical thickness for modulation. Only one layer needs to favor modulation for periodic lateral modulation to be stable in the overall sample. Furthermore, the thin interdiffusion layer below the modulated Al(As)Sb layer in the modulated Set 1 samples may contribute to the modulation. As in the systems described in Li *et al.*, lateral modulation is more likely if the strain in a thin interdiffusion layer is of the same sign as the layer above it.[8]

On the other hand, none of the layers in the Set 2 samples exceed the critical thickness for modulation. Since the two primary layers are an order of magnitude thinner than t_c, even with the influence of the strained interdiffusion layers there is no modulation in these samples.

IV. CONCLUSION

We have investigated the lateral structure of two antimonide superlattices grown on GaSb. We report purely structural lateral modulation in AlSb/AlAs digital-alloy superlattices, but find no modulation in InAs/Al(In)Sb. Both superlattices were grown as buffers in "*W*" quantum well structures intended for room temperature diode lasers. The lateral modulation did not continue into the "*W*" quantum wells grown on the buffer layers, and is therefore not expected to affect the device performance. The modulation is consistent with thermodynamic predictions of the critical thickness for three-dimensional growth in epitaxial layers.

ACKNOWLEDGMENTS

The work at UH was supported in part by the M. Hildred Blewett Scholarship of the American Physical Society, www.aps.org. The work at the Naval Research Laboratory was supported by the Office of Naval Research.

*Corresponding author: rforrest@uh.edu

†Present address: Nanorods LLC, 20271 Goldenrod Land, Suite 2058, Germantown, MD.

‡Present address: Center for Nanoscale Science and Technology, National Institute of Standards and Technology, Gaithersburg, MD 20899.

[1] O. Caha, V. Krapek, V. Holy, S. C. Moss, J. H. Li, A. G. Norman, A. Mascarenhas, J. L. Reno, J. Strangl, and M. Meduna, J. Appl. Phys. **96**, 4833 (2004).

[2] S. T. Chou, K. Y. Cheng, L. J. Chou, and K. C. Hsieh, J. Appl. Phys. **78**, 6270 (1995).

[3] J. M. Millunchick, R. D. Twesten, S. R. Lee, D. M. Follstaedt, E. D. Jones, S. P. Ahrenkiel, Y. Zhang, H. M. Cheong, and A. Mascarenhas, J. Electron. Mater. **26**, 1048 (1997).

[4] J. M. Millunchick, R. D. Twesten, S. R. Lee, D. M. Follstaedt, E. D. Jones, S. P. Ahrenkiel, Y. Zhang, H. M. Cheong, and A. Mascarenhas, MRS Bull. **22**, 38 (1997).

[5]D. W. Stokes, R. L. Forrest, J. H. Li, S. C. Moss, B. Z. Nosho, B. R. Bennett, L. J. Whitman, and M. Goldenberg, J. Appl. Phys. **93**, 311 (2003).
[6]Y. Tang, H. T. Lin, D. H. Rich, P. Colter, and S. M. Vernon, Phys. Rev. B **53**, R10501 (1996).
[7]J. H. Li, D. W. Stokes, O. Caha, S. L. Ammu, J. Bai, K. E. Bassler, and S. C. Moss, Phys. Rev. Lett. **95**, 096104 (2005).
[8]J. H. Li, D. W. Stokes, J. C. Wickett, O. Caha, K. E. Bassler, and S. C. Moss, J. Appl. Phys. **107**, 123505 (2010).
[9]L. E. Shilkrot, D. J. Srolovitz, and J. Tersoff, Phys. Rev. B **62**, 8397 (2000).
[10]A. M. Moy, A. C. Chen, K. Y. Cheng, L. J. Chou, K. C. Hsieh, and C.-W. Tu, J. Appl. Phys. **80**, 7124 (1996).
[11]P. J. Pearah, A.C.Chen, A. M. Moy, K. C. Hsieh, and K. Y. Cheng, IEEE J. Quantum Electron. **30**, 608 (1994).
[12]D. E. Wohlert, K. Y. Cheng, and S. T. Chou, Appl. Phys. Lett. **78**, 1047 (2001).
[13]C. L. Canedy, W. W. Bewley, J. R. Lindle, I. Vurgaftman, C. S. Kim, M. Kim, and J. R. Meyer, App. Phys. Lett. **86**, 211105 (2005).
[14]W. W. Bewley, I. Vurgaftman, C. S. Kim, M. Kim, C. L. Canedy, and J. R. Meyer, Appl. Phys. Lett. **85**, 5544 (2004).
[15]C. L. Canedy, W. W. Bewley, G. I. Boishin, C. S. Kim, I. Vurgaftman, M. Kim, J. R. Meyer, and L. J. Whitman, J. Vac. Sci. Technol. B **23**, 1119 (2005).
[16]C. L. Canedy, W. W. Bewley, C. S. Kim, M. Kim, I. Vurgaftman, and J. R. Meyer, J. Appl. Phys. **94**, 1347 (2003).
[17]G. I. Boishin, C. L. Canedy, I. Vurgaftman, J. R. Meyer, and L. J. Whitman, J. Crystal Growth **286**, 32 (2006).
[18]B. Z. Nosho, W. Barvosa-Carter, M. J. Yang, B. R. Bennett, and L. J. Whitman, Surf. Sci. **465**, 361 (2000).
[19]R. L. Forrest, D. W. Stokes, J. H. Li, R. Lukic, and T. D. Golding, J. Vac. Sci. Technol. B **24**, 1127 (2006).
[20]S. Stepanov and R. Forrest, J. Appl. Cryst. **41**, 958 (2008).
[21]V. Swaminathan and A. T. Macrander, *Materials Aspects of GaAs and InP based Structures* (Prentice Hall, Englewood Cliffs, NJ, 1991).
[22]A. Sasaki, E. R. Weber, Z. Liliental-Weber, S. Ruvimov, J. Washburn, and Y. Nabetai, Thin Solid Films, **367**, 277 (2000).